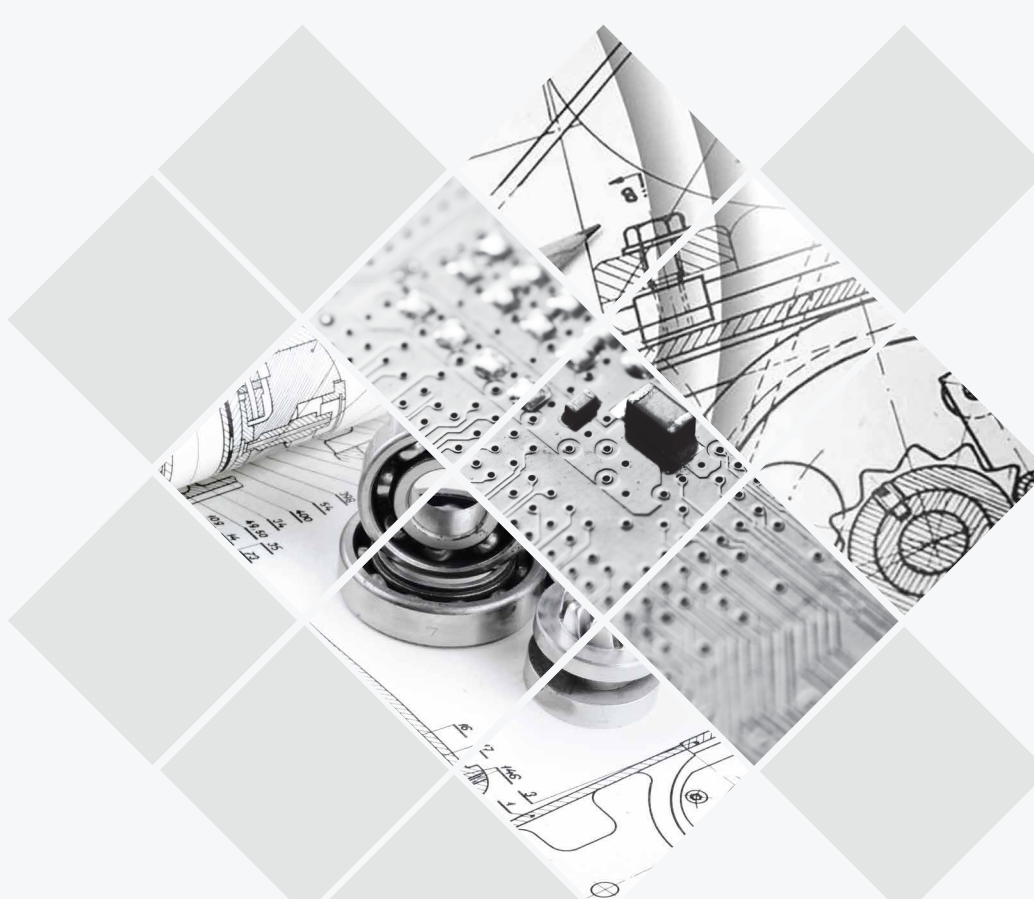


optimization of temperature measurement technique used in high heat flux environment

The heat transfer calculations for turbine flows are known to have a substantial degree of uncertainty. Therefore experimental verification of analytical predictions is needed.



Dmitriy Romanov
Pratt & Whitney Wells,
Maine, USA

Jason Devoe
QuEST Global Services NA, Inc.
Phoenix, Arizona, USA

Lev Ginzursky
LG Tech-Link, LLC
Chandler, Arizona, USA

contents

1.0	Abstract	03
2.0	Introduction	03-04
3.0	Numerical Approach and Boundary Conditions	04-06
4.0	Results and Discussion	06-09
5.0	Conclusions and Recommendations	10
6.0	Nomenclature	10
7.0	References	11
8.0	About QuEST Global	12



Abstract

The heat transfer calculations for turbine flows are known to have a substantial degree of uncertainty [1]. Therefore experimental verification of analytical predictions is needed.

Properly done, metal temperature measurements could inform a designer about the existence of under-cooled or over-cooled locations, suggesting possible opportunities to improve engine thermodynamic and durability characteristics. Operating in a difficult turbine environment, temperature sensors must be well understood to be able to perform the critical task of thermal mapping accurately. The authors analyzed the

influence of factors such as heat flux, sensor positioning, and thermal characteristics of installation assembly on the accuracy of the temperature measured by Crystal Temperature Sensors (CTS) and S-type Thermocouples (TC). The investigation was performed using a numerical simulation of the heat-transfer process taking place in a thin wall with the sensors installed. The recommendations drawn from this experience should help analytical designers and instrumentation engineers optimize experimental techniques and improve the quality of engine test result interpretation.

Introduction

The search for the optimum balance between turbine thermodynamic efficiency and durability characteristics is central to the process of engine development.

Today, sophisticated analytical tools provide powerful support to design engineers. At the same time these tools are unable to overcome their semi-empirical nature when calculating heat-transfer coefficients. The main contributor to this problem is the complexity of the turbine gas flow which is characterized by blade-vane interaction effects, boundary layer transition, separation and non-isothermal mixing. It is difficult, if not impossible, to come up with a thorough analytical definition of these processes.

The resulting uncertainties in metal temperature calculations prevent engineers from basing important design decisions purely on analytical predictions. That is why comprehensive metal temperature validation testing becomes an essential part of modern engine development.

There are a number of temperature measurement techniques that could be used to perform thermal mapping of critically important turbine parts. They compete with each other on their ability to operate in a hostile turbine environment cost effectively with good accuracy.

This investigation focuses on the thermocouple and crystal temperature sensor technologies because of their promising record of achievement in all three categories.

Thermocouples have a long history of application and do not require an introduction. CTS is a relatively new arrival [2, 3, 4] with a distinctly different principle of operation. It is based on the phenomenon of irradiation induced SiC crystal lattice expansion, followed by the relieving of the expanded lattice structure during annealing. The sensor is embedded into a part, where it will be subjected to the turbine test environment. After the CTS is removed, changes in crystal structure characteristics are measured and related to the temperature experienced by the sensor. The miniature size and wireless installation of CTS allows for a high density of instrumentation, which has proven to be helpful in the engine development process [5, 6].

As with any instrumentation used in the validation procedure, both techniques must demonstrate high accuracy not only in the laboratory setting but in real engine conditions as well. This means that the technological and environmental factors potentially able to affect the accuracy of temperature measurement should be studied and recommendations should be made to refine the methodology of sensor application.

In this particular case study a thin intensely air-cooled wall made of Ni-based super-alloy, with and without thermal barrier coating (TBC) was chosen to represent a typical element of such critical turbine parts as blades, nozzle vanes, air seals, and combustor liners. The objective of this investigation was to evaluate systematic errors caused by the local thermal disturbance associated with temperature sensor installation in a high heat flux environment. Among the factors considered: heat flux level, sensor installation layout, and variations

in the thermo-physical properties of the materials used for installation.

Similar parametric studies [7, 8, 9, 10] have been performed for a range of heat loads and sensor installation techniques not characteristic for modern turbine environments. This current work was undertaken to improve understanding of the temperature measurement process and to contribute to the further development of turbine experimental techniques.

Numerical Approach and Boundary Conditions

Geometric models

The model used for this study was as follows: an S-type Thermocouple (TC) and Crystal Temperature Sensor (CTS) were installed into a thin wall of the same geometry, made of the same material and exposed to the same thermal boundary conditions. The wall thickness was 1.0mm and the thermal barrier coating (TBC), when applied, increased the wall thickness by an additional 0.2mm. It was expected that the installation of the sensors would deform the original temperature field in the wall and potentially cause measurement errors. This investigation focused on the heat-transfer steady-state process that takes place in the geometric domain embracing the metallic wall – sensor – assembly filler system. The effect of thermal conduction along the TC thermo-electrode wires was not modeled due to its strong dependency on individual design features.

Embedded S-type Thermocouple

A typical TC installation, based on NASA experience [11], is shown in Figure 1. A 0.61 mm wide and 0.58 mm deep groove was cut into the wall in such a way that it would comfortably accommodate the TC assembly packed into a 0.51 mm diameter protective platinum shell, which could be secured in place by using welding and metal filler or ceramic based thermo-cement. In both cases, at the end of the installation process, the outer surface of the instrumented part was returned to its original aerodynamic shape. A gap on the order of 0.05 mm around the platinum shell perimeter was introduced

to account for manufacturing tolerances. It is important to note that when cement is used as the filler, this gap should not contain any air pockets. On the contrary, the other technique cannot produce consistent metallic filler penetration. Air trapped in the gap is a potential source of systematic temperature measurement errors and was considered in our study as a factor of influence. The six levels of metallic filler penetration are defined in terms of the size of the cross sectional area of the air pocket ranging from 25% to 81%.

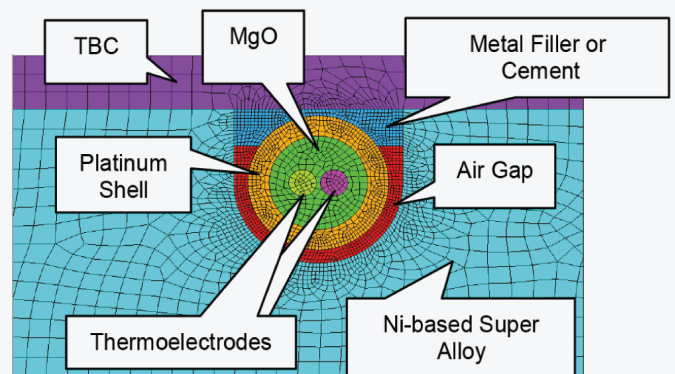


Figure 1A. TC Installation Computational Domain

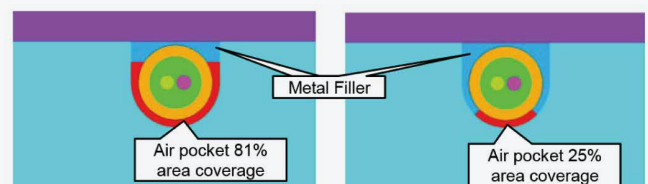


Figure 1B. TC With Various Metallic Filler Coverage Scenarios



Crystal Temperature Sensor

A CTS has a rectangular prism shape with the dimensions of 0.20x0.20x0.38 mm. It was installed into a wall cavity with a 0.71 mm diameter and a depth of 0.64 mm (shown in Figure 2-A, B, C). In all three installation configurations the sensor is depicted as being positioned at the bottom of the cavity and secured in place by thermo-cement. Two other CTS positions were also considered with a 0.10mm and 0.23 mm. distance between the bottom of the cavity and the lower CTS surface. As an additional measure of security a 0.05 mm thick, 1.52 mm diameter metal shim was spot-welded over the top of the cavity (Figure 2-B). This is often recommended for long duration, multi-cycle engine tests.

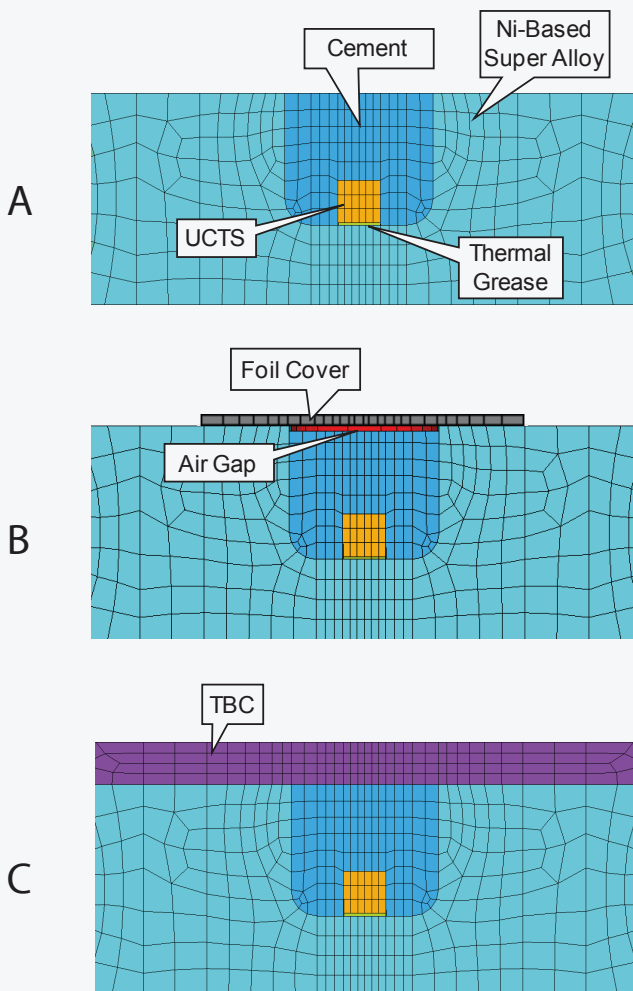


Figure 2. CTS Installation Configurations

Operating conditions and material properties

Thermo-physical characteristics for all elements of the wall – sensor – assembly filler system are listed in TABLE 1.

TABLE 1.

Elements of Sensor Installation Assembly	K - Thermal Conductivity Coefficient [W/m- °C]	Comments
CTS sensor (irradiated SiC)	20	From [12]
Thin wall (Ni-based Super-Alloy)	26	From [13]
TBC coating	1	Zirconia, From [14]
CTS thermo-cement	0.6	Resbond 919
CTS Buffer Layer	1.4	Silica
TC thermo-electrode	38	Platinum/Rhenium
TC two-hole ceramic tubing	0.6	MgO
TC metallic filler	16.9	Chromel
TC protective shell	88	Platinum
TC ceramic filler	1.4	Sauereisen #8

To better simulate turbine engine operating conditions the following assumptions were made:

- Reference Point Parameters were taken from a NASA Report [13]
- Ref. Point Heat Flux was assumed to be 75% of (H.F.) max for the metal wall without TBC application
- All Ref. Point Parameters (see TABLE 2) except Hc.air side were kept constant for all configurations and regime points
- Heat Flux variations from 0% to 100% were achieved by corresponding adjustments to the H c. air side only
- A series of calculations made for the undisturbed thin wall (with and without TBC) under the chosen boundary conditions resulted in the graph shown in Figure 3, which depicts the heat-transfer operational domain considered in this study.

TABLE 2. Reference Point Boundary Conditions [13]

Ref. Parameter	Value	Comments
Tgas	1739.4 °C	Kept constant
Tc. air	696.1 °C	Kept constant
Hgas	5252.7 W/m ² - °C	Kept constant
Hc. air	7183.4 W/m ² - °C	Variable

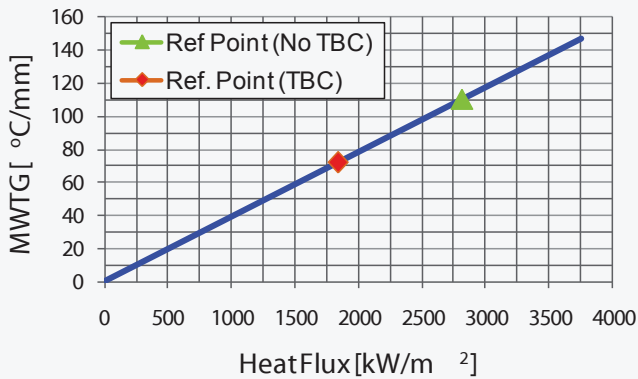


Figure 3. Heat Flux Boundary Conditions

Numerical modeling was performed using 3D FEA ANSYS code with the following methodology:

- Temperatures measured (t_m) by sensors were taken at the geometrical center of a TC junction or CTS rectangular prism

- Temperatures, which ideally should be measured (t_u), were taken at exactly the same locations from the runs simulating the heat-transfer process in the wall undisturbed by the sensor installation
- Value of $\theta = \frac{t_u - t_m}{t_u} \times 100\%$ was used as a measure of the Temperature Read Error
- Metal Wall Temperature Gradients $MWTG = \frac{t_w.mh - t_w.mc}{\delta}$ were calculated for the undisturbed metal wall
- The TC study was focused on the assessment of systematic errors associated with the quality of the thermal contacts and the variations in thermal properties of the materials used in the TC installation assembly in close vicinity to the measuring junction without considering the effect of heat flow along the lead wires.

Results and Discussion

The visualization of the simulation results shown in Figures 4-7 for TC installation and in Figures 12-14 for CTS, clearly indicate that the presence of the sensor embedded into the thin wall under the chosen operating conditions caused a noticeable distortion of the original temperature field. The extent of the influence of sensor installation on the temperature field did not go beyond ± 1 caliber, where a caliber is the size of the trench or cavity depending on which type of sensor was used. It was found that the particulars of the installation techniques and differences in the thermal characteristics of the materials used were the most influential factors. Due to the specifics of each sensor installation the results had to be analyzed separately.

Thermocouple embedded into the thin wall

Multiple runs were performed to simulate various installation and regime scenarios. Figures 4, 5, 6, and 7 show several examples of the visualization outputs of these runs. Each of these are a combined image in which half the temperature field shows an undisturbed thin wall and the other half shows how the temperature field was distorted by a particular installation scenario. The specific examples pictured below simulate just one reference point heat load regime, which was characterized by the value of the $MWTG = 73.3$ oC/mm for the TBC applied case, and $MWTG = 111$ oC/mm for the case without TBC.

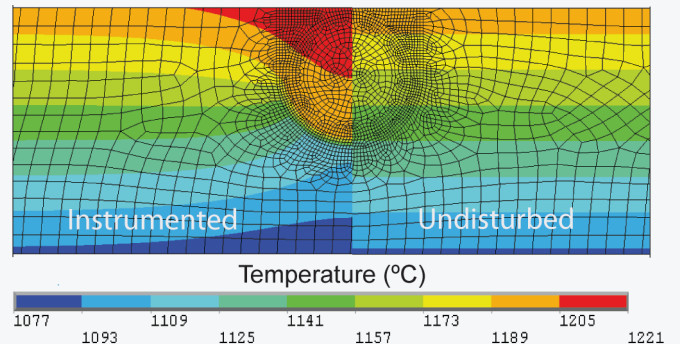


Figure 4. No TBC, HFRP, Metallic Filler, 50% Air GAP

Figures 4 and 5 both had the same amount of Metallic Filler penetration (50% Air Gap). The only difference is that Figure 5 had a layer of TBC applied, and Figure 4 did not.

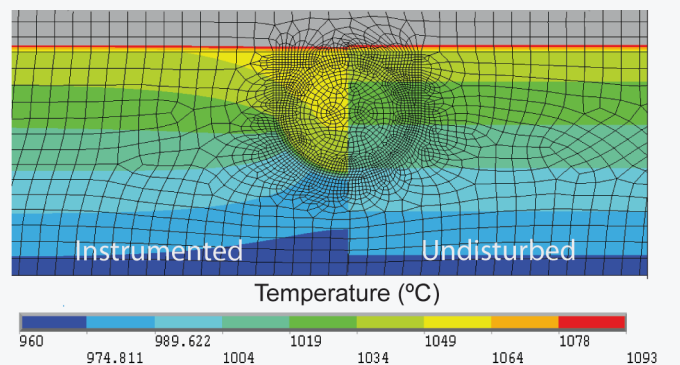


Figure 5. TBC Applied, HFRP, Metallic Filler, 50% Air GAP



Similarly Figures 6 and 7 exemplify the cases in which Ceramic Filler was used. Once again, the only difference is that one case had a TBC layer (Figure 7.) and one did not (Figure 6.).

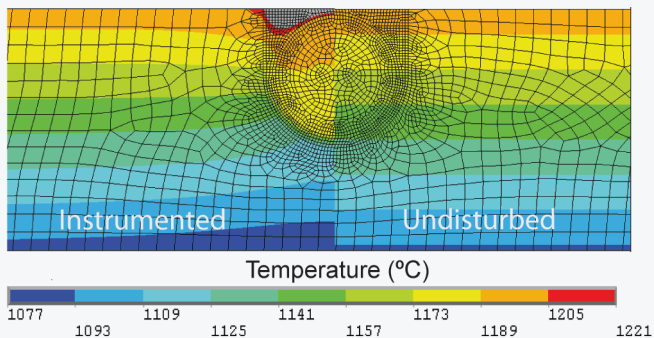


Figure 6. No TBC Applied, HFRP, Ceramic Filler

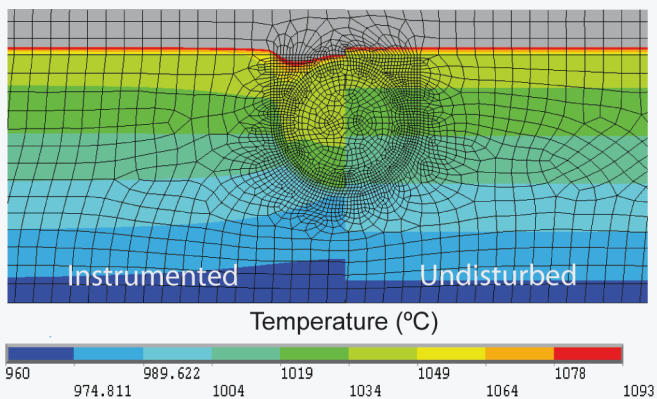


Figure 7. TBC Applied, HFRP, Ceramic Filler

These pictures should compliment the study of the quantative results which are presented in the graphs (Figures) below.

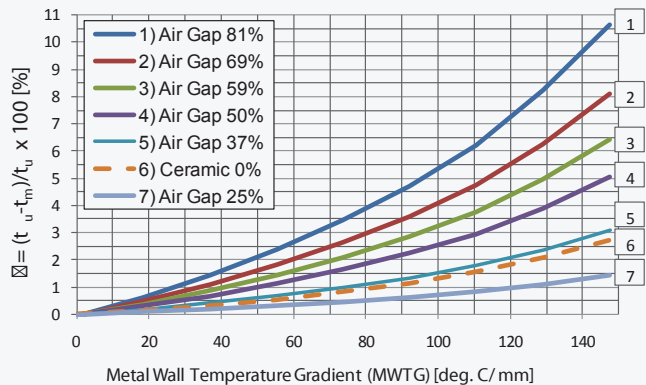


Figure 8. TC, No TBC. Read Error Vs Mwtg

As shown in Figure 8. for the 'No TBC' metallic filler cases the temperature measurement error increased with the heat load and air gap values. In the worst case scenario with maximum air gap percentage and 100% heat load the temperature measurement error reached ~10%. The ceramic filler case (depicted as a dotted line) differed from the other because of the absence of an air gap. In the worst case scenario for this particular case the maximum error for the same heat load dropped to ~3%.

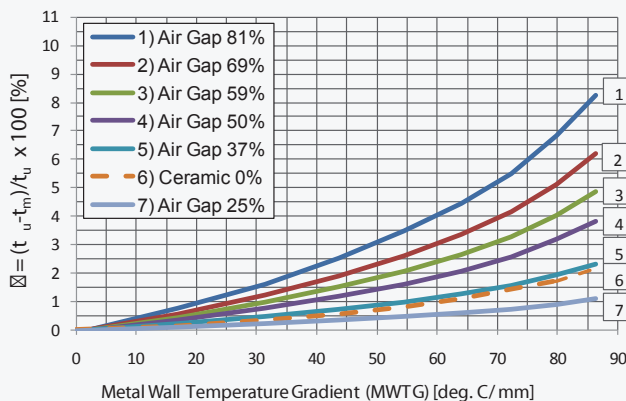


Figure 9. TC, WITH TBC. Read Error Vs Mwtg

Figure 9. shows the same pattern of behavior for the TBC coated wall. The level of maximum error reached here was substantially lower than in Figure 8, which should be attributed to the fact that with coating protection the same aero-thermo boundary conditions will produce smaller heat flux and smaller metal wall temperature gradients.

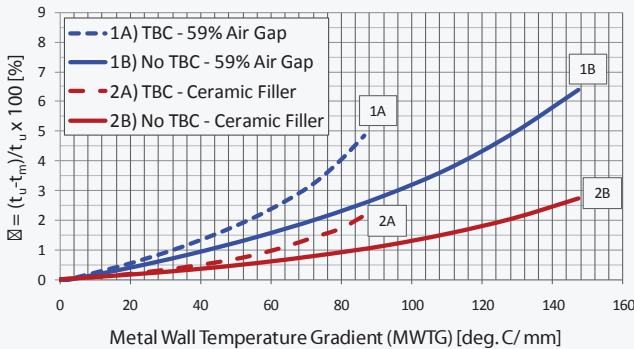


Figure 10. TC Read Error Vs. Mwtg

In Figure 10 a direct comparison is made between typical cases with and without TBC. The blue dash curve represents a case with metallic filler and a 59% air gap that had TBC applied to its surface. The solid blue curve had the exact same level of metallic filler penetration and air gap, but did not have TBC.



The curves in red represent the ceramic cases. The dotted line shows a case in which TBC was applied, while the solid line shows a case in which no TBC was applied. It should be noted that a more aggressive trend was shown by cases with TBC; confirming that in these cases the temperature field distortion in the vicinity of the TC Bead was greater.

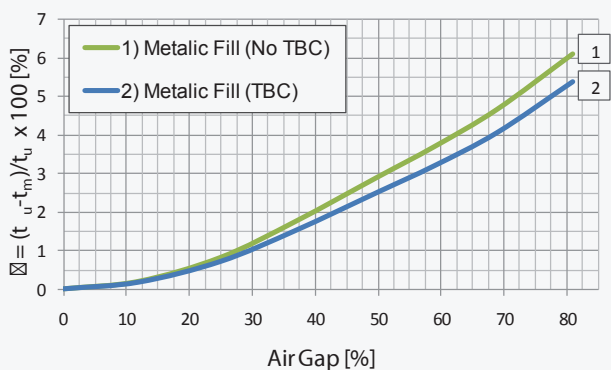


Figure 11. TC Read Error Vs. Air GAP, HFRP

Finally, Figure 11. gives an assessment of the temperature error dependency on the level of weld filler penetration. All of the information presented in Figure 11 is for one set of boundary conditions, which was chosen as the Reference Point.

CTS Embedded into Thin Wall

Crystal Temperature Sensor installation techniques are simple and easy to control. In the absence of lead wires there is no need to estimate the potential systematic errors associated with heat conduction through the wires. As a result, this investigation focused solely on the quality of thermal contact between the sensor and surrounding elements of the installation assembly. The main factors considered were heat load, position of the sensor inside the cavity and thermal conductivity of the filling cement. All of these factors were considered for the three CTS installation configurations depicted in Figure 2.

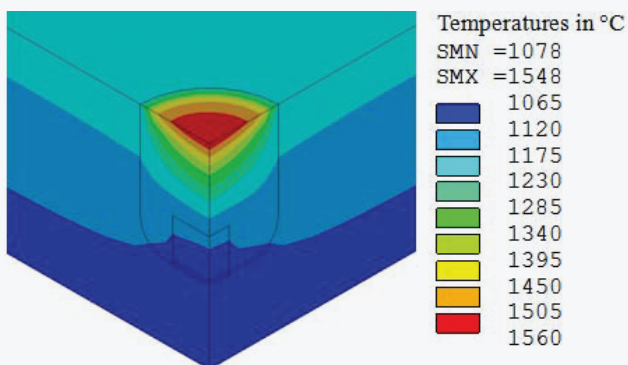


Figure 12. CTS Configuration A, HFRP, k=.6 [W/m-deg. C]

Resulting temperature distributions are presented in Figures 12-14 for the heat load corresponding to the reference point boundary conditions and thermo conductivity of the Resbond 919 cement used as a filler. The temperature field distortion due to the presence of CTS in each of the configurations was symmetrical in relation to the axis of the cavity, penetrating the whole wall thickness, and its propagation in radial directions was limited to approximately 2xD, where D is the cavity diameter.

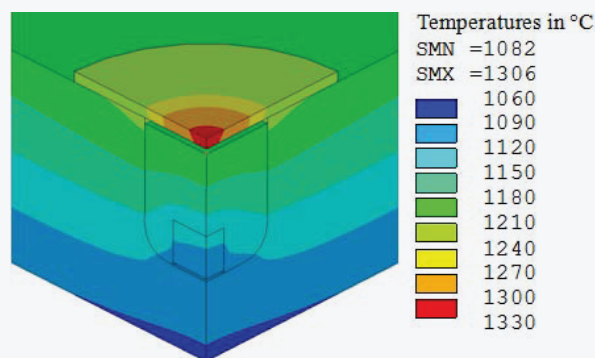


Figure 13. CTS Configuration B, HFRP, k=.6 [W/m-deg. C]

In Configuration B (Figure 13) a thin piece of metal shim was spot welded over the top of the cavity as a measure of additional security. The worst case scenario was assumed for these cases, meaning that there was a small air pocket (0.03 mm) between the ceramic filler and the shim and that the spot welds were placed in such a way that they did not allow gas circulation.

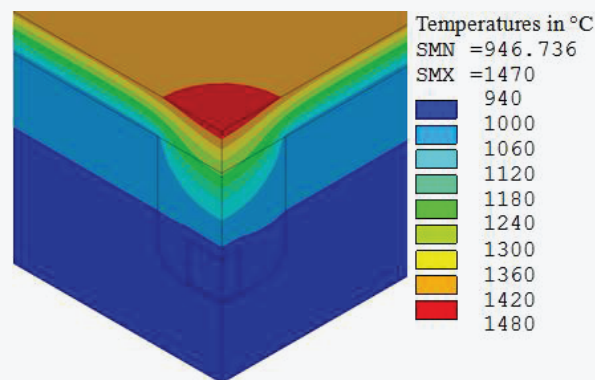


Figure 14. CTS Configuration C, HFRP, k=.6 [W/m-deg. C]

Figures 15-17 give a quantitative assessment of the heat load influence on measurement error for the three progressively increasing values of k (filling cement thermo conductivity). Each installation configuration had its own range of θ variations but all of them demonstrated the same trend of increasing systematic error with an increase in MWTG and a decrease in thermal conductivity.

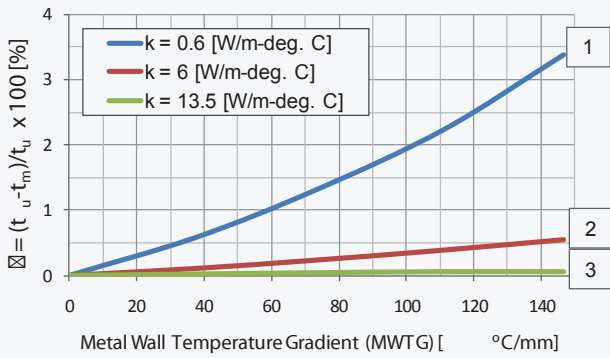


Figure 15. CTS Configuration – A

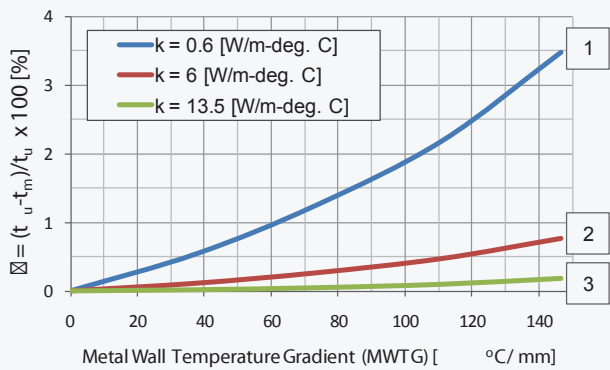


Figure 16. CTS Configuration - B

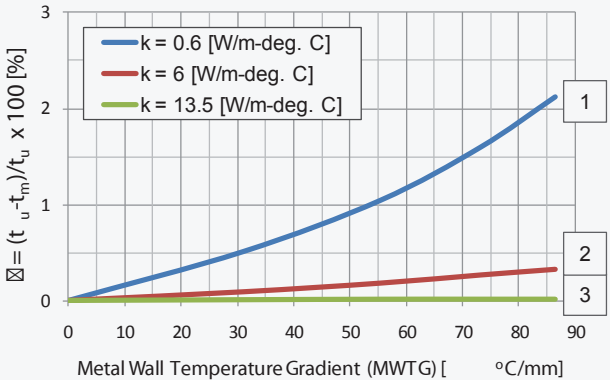


Figure 17. CTS Configuration - C

Apparently the presence of air trapped in the pocket of configuration B made local thermo resistance of the installation assembly greater causing an elevation of the maximum error. The logic behind the decrease of the maximum error level for Configuration C was of a different nature. Existence of the 0.20 mm TBC layer on top of the metal wall moderated the heat load, bringing the max MWTG from 147.5 down to 86.4.

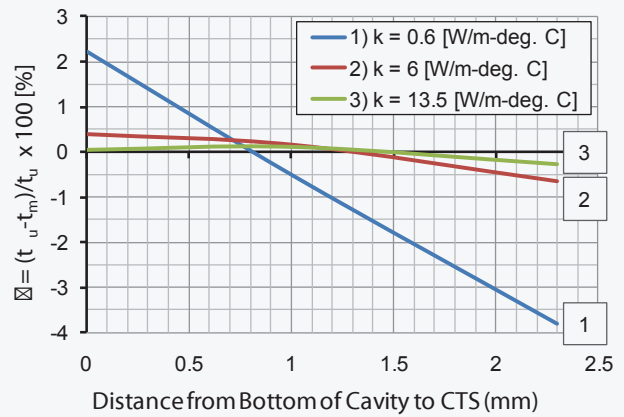


Figure 18. CTS Configuration – A, HFRP

CTS position in the cavity, as a factor of influence, is examined in Figure 18. It shows that placing the sensor in a ‘sweet spot’ position could reduce the systematic error for all configurations.

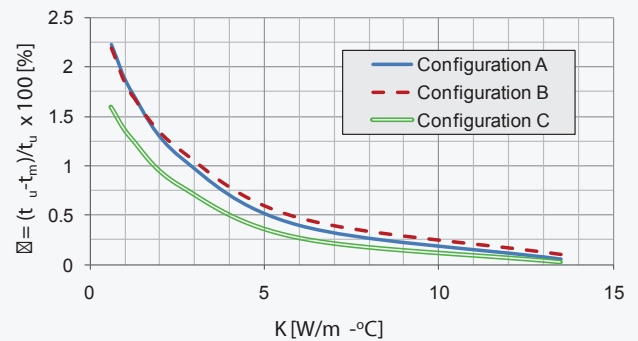


Figure 19. CTS Located on The Bottom, HFRP

Finally, Figure 19 shows that an improvement in the thermal conduction characteristics of the cement could sharply decrease temperature measurement errors.



Conclusions and Recommendations

On the basis of the information obtained during the course of this investigation the following conclusions could be drawn.

1. Finite Element Analysis is an effective tool for calculating systematic temperature measurement error as long as exact boundary conditions, geometric and thermo physical parameters of sensor installation assembly are known.
2. Uncooled or lightly cooled turbine stage parts characterized by low level temperature gradients could be instrumented with both types of sensors without fear of substantial systematic temperature measurement error.
3. Starting from $MWTG \approx 44.4$, the value of θ could become too high to ignore and an Ansys-type simulation of the heat transfer situation should become a routine part of the thermal mapping data reduction process. To ensure good calculation results some measures should be taken to guarantee that the characteristics of the sensor installation assembly are consistent and predictable.

4. With the existing trend in turbine design, it is expected that the operating point will move to the high end of the MWTG and consequently θ . To bring errors to a manageable level, the industry needs to develop an installation technique which will be less sensitive to factors of influence found in this study. The use of thermo cement with higher thermo conductivity, and the elimination of air pockets in the installation assembly are two ways in which an improvement could be made.

The results of this study provide insight on how variables associated with installation can affect the accuracy of the sensors studied. However, in order to get a broader understanding it is highly recommended that additional studies be done into how these factors of influence affect the accuracy of thermocouples and CTS when unsteady state conditions are considered.

Nomenclature

A, B, C	CTS installation configurations shown in Figure 2
BC	Boundary Conditions shown in TABLE 2
D	CTS cavity diameter, mm
H	Heat transfer coefficient, $W/m^2 \cdot ^\circ C$
HFRP	Heat Flux calculated for the Reference Point BC
t	temperature, $^\circ C$
TBC	Thermal Barrier Coating
TC	Thermocouple
k	Thermal conductivity, $W/m \cdot ^\circ C$
$MWTG = \frac{t_{w.mh} - t_{w.mc}}{\delta}$	metal wall temperature gradient, $^\circ C/mm$
CTS	Crystal Temperature Sensor
δ	Thickness, mm
$\theta = \frac{t_u - t_m}{t_u} \times 100\%$	Normalized temperature measurement error, %

Subscripts

c.air	cooling air
gas	hot gas
m	measured (at the sensor geometrical center)
u	undisturbed (taken at the same depth as "m")
w	wall
w.c.	air wall cooling air side
w.g	wall hot gas side
w.mh	wall metal hot side
wmc	wall metal cold side



References

1. Brunner, M.H., Rose, M.G., Mühlbauer, K., and Abhari, R.S. 2008. "In-situ heat transfer measurements on coated and uncoated turbine blades of a full-scale turbine". Proceedings of the Institution of Mechanical Engineers, Part A: Journal of Power and Energy, 222 (3), pp. 331-338.
2. Nikolaenko, V. A., Morosov, V. A., and Kasianov, N. I., 1976. "Crystal Maximum Temperature Measurer for Special Applications". Rev. Int. Htes Temp. et Refract, 13, pp. 17-20.
3. Ginzburzsky, Lev. 2009. "Crystal Temperature Sensor Technology". 33rd Annual Conference on Composites, Materials.
4. Ginzburzsky, Lev, 2010. "UCTS, How it Works". <http://www.lgtechlink.com>
5. Shukin, Sergey, Annerfeldt, Mats, Bjorkman, Mats. 2008. "Siemens SGT-800 Industrial Gas Turbine Enhanced to 47MW. Design Modifications and Operation Experience". ASME Turbo Expo 2008: Power for Land, Sea, and Air, GT2008-5008, 7, pp. 65-70.
6. Annerfeldt, M., Shukin, S., Bjorkman, M., Karlsson, A., Jonsson, A., and Svistounova, E. 2004. "GTX 100 Turbine Section Measurement Using a Temperature Sensitive Crystal Technique. A Comparison with 3D Thermal and Aerodynamic Analysis". PowerGen Europe, Barcelona.
7. Bileka, B.D., 1998. "Metodicheskie Osobennosti Primenenia Cristallicheskikh izmeritelei Maksimalnikh Temperatut pri Provedenii Termometrirovania DetaleiGazovikh Turbin". Prom. Teplotekhnika, 20 (5).
8. Attia, M.H., and Kops, L. February 1988. "Distortion in Thermal Field Around Inserted Thermocouples in Experimental Interfacial Studies - Part II: Effect of the Heat Flow Through the Thermocouple". Journal of Engineering for Industry, 110.
9. Xu, F., Gadala, M.S., 2005. "Investigation of error sources in temperature measurement using thermocouples in water impingement cooling". Experimental Heat Transfer, 18(3), pp. 153-177.
10. Kuznetsov, G.V., and Mukhammadeev, K.M., 2010. "Numerical Estimation of Errors of Temperature Measurements by Thermocouples Using Special Glues and Pastes". Journal of Engineering Thermophysics, 19(1).
11. Holanda, R., Glawe, G.E., and Krause, L.N., May 1974. "Miniature sheathed thermocouples for turbine blade temperature measurement". NASA TN D-7671.
12. Youngblood, G.E., Senior, D.J., Moore, C.E., Trimble, D.J., June 1996. "Effects of Neutron Irradiation on Thermal Conductivity of SiC-Based Composites and Monolithic Ceramics".
13. Halila, E.E., Lenahan, D.T., and Thomas, T.T. June 1982. "High Pressure Turbine Test Hardware Detailed Design Report". NASA-CR-167955.
14. Lee, D.H., Kim, K.M., Shin, S. and Cho, H.H., 2009. "Thermal Analysis in a Film Cooling Hole with Thermal Barrier Coating". Journal of Thermophysics and Heat Transfer, 23 (4).



About QuEST Global

QuEST Global is a focused global engineering solutions provider with a proven track record of over 17 years serving the product development & production engineering needs of high technology companies. A pioneer in global engineering services, QuEST is a trusted, strategic and long term partner for many Fortune 500 companies in the Aero Engines, Aerospace & Defence, Transportation, Oil & Gas, Power, Healthcare and other high tech industries. The company offers mechanical, electrical, electronics, embedded, engineering software, engineering analytics, manufacturing engineering and supply chain transformative solutions across the complete engineering lifecycle.

QuEST partners with customers to continuously create value through customer-centric culture, continuous improvement mind-set, as well as domain specific engineering capability. Through its local-global model, QuEST provides maximum value engineering interactions locally, along with high quality deliveries at optimal cost from global locations. The company comprises of more than 7,000 passionate engineers of nine different nationalities intent on making a positive impact to the business of world class customers, transforming the way they do engineering.



BORN TO ENGINEER

<http://quest-global.com>